Y-Shaped Amphiphilic Brushes with Switchable Micellar Surface Structures

ARTICLE *in* JOURNAL OF THE AMERICAN CHEMICAL SOCIETY · JANUARY 2004

Impact Factor: 12.11 · DOI: 10.1021/ja038051u · Source: PubMed

5 AUTHORS, INCLUDING:

Eugene R Zubarev
Rice University
91 PUBLICATIONS **3,541** CITATIONS

SEE PROFILE

J|A|C|S
ARTICLES
Published on Web 11/26/2003

Y-Shaped Amphiphilic Brushes with Switchable Micellar Surface Structures

Duangrut Julthongpiput, Yen-Hsi Lin, Jing Teng, Eugene R. Zubarev,* and Vladimir V. Tsukruk*

Contribution from the Department of Materials Science & Engineering, Iowa State University, Ames, Iowa 50011

Received August 21, 2003; E-mail: zubarev@iastate.edu; vladimir@iastate.edu

Abstract: We observed novel nanoscale surface structures of segregated pinned micelles and craterlike micelles formed by grafted Y-shaped molecules and their reversible reorganization in selective solvents. The Y-shaped molecules have two incompatible polymer chains (polystyrene and poly(*tert*-butyl acrylate)) attached to a functional stemlike segment capable of covalent grafting to a functionalized silicon surface. Postgrafting hydrolysis of poly(*tert*-butyl acrylate) arms imparts amphiphilicity to the brush. We demonstrated that spatial constraints induced by a chemical junction of two relatively short (6−10 nm) dissimilar arms in such Y-shaped molecules lead to the formation of segregated micellar surface nanostructures in the grafted layer. We proposed a model of these segregated pinned micelles and the corresponding reverse micelles (craterlike structures) featuring different segregation states of hydrophobic polystyrene and hydrophilic poly(acrylic acid) arms. The arms undergo conformational rearrangements in selective solvents in a controlled and reversible fashion. These nanoscale structural reorganizations define adaptive macroscopic wetting surface properties of the amphiphilic Y-shaped brushes. This surface structure and switchable behavior can be considered as a promising way toward the patterning of solid substrates with adaptive nanowells, which could be used for trapping of adsorbing nanoscale objects.

Introduction

Functionalized interfacial organic and polymer layers fabricated from molecular segments with different amphiphilicity can be designed to act as a "smart" or switchable surface.[1] These surfaces are capable of responding to very subtle changes in the surrounding environment such as pH,[2] surface pressure,[3] temperature,[4] light,[5] and solvent quality.[6−8] The macroscopic responses are caused by the reorganization of the internal or surface structure of the grafted layers. This reorganization is responsible for controlling physical properties important in applications of colloid stabilization,[9] drug delivery and biomimetic materials,[10,11] chemical gates,[12] protein adsorption,[13] and tuning nanotribological properties for tailored surfaces.[14−16] Surface composition and, hence, the surface energy, adhesion, friction, and wettability can be "tuned" to a desired physical state. This provides a means for the fabrication of "smart surfaces" with new sophisticated properties such as self-cleaning and self-refreshing abilities or superhydrophobic behavior.[17,18] Such surfaces hold great promise in the design of nanoelectromechanical, bioanalytical, and microfluidic devices with adaptive properties.[19−24]

Stimuli-responsive surface polymer layers can be designed by using a variety of approaches including the reversible

(1) (a) Kato, K.; Uchida, E.; Kang, E.-T.; Uyama, Y.; Ikada, Y. *Prog. Polym. Sci.* **2003**, *28*, 209−259. (b) Milner, S. T. *Science* **1991**, *251*, 905−914.
(2) Israëls, R.; Leermakers, F. A. M.; Fleer, G. J.; Zhulina, E. B. *Macromolecules* **1994**, *27*, 3249−3261.
(3) (a) Tsukruk, V. V.; Genson, K. L.; Peleshanko, S.; Markutsya, S.; Greco, A.; Lee, M.; Yoo, Y. *Langmuir* **2003**, *19*, 495−499. (b) Lee, M.; Kim, J.-W.; Yoo, Y.-S.; Peleshanko, S.; Larson, K.; Vaknin, D.; Markutsya, S.; Tsukruk, V. V. *J. Am. Chem. Soc.* **2002**, *124*, 9121−9128.
(4) Takei, Y. G.; Aoki, T.; Sanui, K.; Ogata, N.; Sakurai, Y.; Okanao, T. *Macromolecules* **1994**, *27*, 6163−6166.
(5) (a) Hall, R.; Hara, M.; Knoll, W. *Langmuir* **1996**, *12*, 2551−2555. (b) Dante, S.; Advincula, R.; Frank, C. W.; Stroeve, P. *Langmuir* **1999**, *15*, 193−201. (c) Ichimura, K.; Oh, S.-K.; Nakagawa, M. *Science* **2000**, *288*, 1624−1626. (d) Siewierski, L. M.; Brittain, W. J.; Petras, S.; Foster, M. D. *Langmuir* **1996**, *12*, 5838−5844. (e) Tsukruk, V. V.; Bliznyuk, V. N. *Prog. Polym. Sci.* **1997**, *22*, 1089−1132. (f) Sidorenko, A.; Houphouet-Boigny, C.; Villavicencio, O.; McGrath, D. V.; Tsukruk V. V. *Thin Solid Films* **2002**, *410*, 147−158.
(6) (a) Auroy, P.; Auvray, L.; Leger, L. *Phys. Rev. Lett.* **1991**, *66*, 719−722. (b) Grest, G. S.; Murat, M. *Macromolecules* **1993**, *26*, 3108−3117.
(7) Raviv, U.; Tadmor, R.; Klein, J. *J. Phys. Chem. B* **2001**, *105*, 8125−8134.
(8) Tsukruk, V. V. *Adv. Mater.* **2001**, *13*, 95−108.
(9) Pincus, P. *Macromolecules* **1991**, *24*, 2912−2919.
(10) Galaev, I. Y.; Mattiasson, B. *Trends Biotechnol.* **1999**, *17*, 335−340.
(11) Aksay, I. A.; Trau, M.; Manne, S.; Honma, I.; Yao, N.; Zhou, L.; Fenter, P.; Eisenberger, P. M.; Gruner, S. M. *Science* **1996**, *273*, 892−898.
(12) Ito, Y.; Ochiai, Y.; Park, Y. S.; Imanishi, Y. *J. Am. Chem. Soc.* **1997**, *119*, 1619−1623.
(13) Ornatska, M.; Jones, S. E.; Naik, R. R.; Stone, M.; Tsukruk, V. V. *J. Am. Chem. Soc.* **2003**, *125*, 12722.
(14) Leger, L.; Raphaël, E.; Hervert, H. *Adv. Polym. Sci.* **1999**, *138*, 185−225.
(15) (a) Ruths, M.; Johannsmann, D.; Rühe, J.; Knoll, W. *Macromolecules* **2000**, *33*, 3860−3870. (b) Bliznyuk, V. N.; Everson, M. P.; Tsukruk, V. V. *J. Tribol.* **1998**, *120*, 489−495.
(16) (a) Mansky, P.; Liu, Y.; Huang, E.; Russell, T. P.; Hawker, C. *Science* **1997**, *275*, 1458−1460. (b) Belge, G.; Beyerlein, D.; Betsch, C.; Eichhorn, K.; Gauglitz, G.; Grundkle, K.; Voit, B. *Anal. Bioanal. Chem.* **2002**, *374*, 403−411.
(17) Blossey, R. *Nat. Mater.* **2003**, *2*, 301−306.
(18) Lafuma, A.; Quere, D. *Nat. Mater.* **2003**, *2*, 457−460.
(19) Graighead, H. G. *Science* **2000**, *290*, 1532−1535.
(20) Jacobs, H. O.; Tao, A. R.; Schwartz, A.; Gracias, D. H.; Whitesides, G. M. *Science* **2002**, *296*, 323−325.
(21) Tsukruk, V. V. *Prog. Polym. Sci.* **1997**, *22*, 247−311.
(22) (a) Jones, D. M.; Smith, J. R.; Huck, W. T.; Alexander, C. *Adv. Mater.* **2002**, *14*, 1130−1134. (b) Ista, L. K.; Perez-Luna, V. H.; Lopez, G. P. *Appl. Environ. Microbiol.* **1999**, *65*, 1603−1609.
(23) Nath, N.; Chilkoti, A. *Adv. Mater.* **2002**, *14*, 1243−1247.

10.1021/ja038051u CCC: $25.00

photoisomerization reaction, reversible swelling/collapse of water-soluble grafted polymers, and phase separation in binary grafted brushes or diblock copolymers.[1−8] Polymer brushes composed of flexible polymer chains tethered to a solid substrate are a subject of intensive theoretical and experimental investigations.[25−27] Recent sophisticated designs resulted in the preparation of surface polymer layers with unique adaptive properties. For instance, reversible switching of surface properties has been recently observed for mixed, binary brushes grafted to a solid substrate.[28−30] For these systems, different conformational changes of dissimilar polymer chains A and B with high molecular weights randomly tethered to a solid surface resulted in dramatic structural reorganization. It has been shown that the shifts in the balance of lateral and vertical phase separations of dissimilar polymer chains with segregated regions measuring 10−300 nm across are responsible for this phenomenon.[31,32]

However, to date, the type of surface structures formed in binary brushes under conditions of spatial constraints imposed by their chemical connection to a single grafting site (so-called Y-shaped molecules) has not been explored due to synthetic limitations. According to recent theoretical predictions, such molecules should form a wide variety of segregated layers with various micellar surface structures controlled by chemical attachment, grafting density, and composition of chains A and B.[33,34] The formation of pinned, mixed, internally segregated, and split micelles, as well as striped morphology, on the nanometer scale was predicted. Variation of the morphology with grafting density, molecular weight of brushes, and composition has been discussed in detail by Zhulina and Balazs.[33] The full phase diagram was calculated, which suggested a rich polymorphism in Y-shaped grafted molecules.

In a search for the variety of switchable nanoscale surface structures and in accordance with these theoretical predictions, we designed a novel type of Y-shaped copolymer[35] combining two dissimilar polymer chains (polystyrene (PS) and poly(*tert*-butyl acrylate) (PBA)) attached to a single focal point capable of chemical grafting to a silicon surface (Figure 1). The binary brushes containing hydrophobic and hydrophilic chains confined to a single grafting site were prepared via postgrafting hydrolysis of the PBA arms and contained amphiphilic grafted molecules with different volume ratios of PS and poly(acrylic acid) (PAA) arms.

In this study, we focused on molecules with two different compositions of flexible arms with approximately a 60:40 (brushes **1** and **2**) and a 50:50 (brush **3**) PS:PAA volume ratio (Table 1). Our preliminary results for similar molecules showed the formation of unusual surface nanostructures for brushes **1** and **2**.[36] Here, we report the complete results of comprehensive studies of the nanoscale surface structures of a wide variety of Y-shaped molecules representing internally segregated pinned micelles and craterlike micelles of grafted molecules with different molecular weights and composition of polymer arms and their reversible structural reorganization upon treatment with selective solvents.

Table 1. Surface Properties of the Y-Shaped Brush Layer[a]

brush	film thickness (nm)	RMS roughness (nm)	grafting density[b] Σ (chain/nm^2)	grafting distance[b] D (nm)
1	1.96 ± 0.20	0.25 ± 0.02	N/A	N/A
1′	1.35 ± 0.20	0.37 ± 0.03	0.10	3.6
2	2.02 ± 0.10	0.26± 0.02	N/A	N/A
2′	1.96 ± 0.10	0.72 ± 0.14	0.15	3.0
3	2.75 ± 0.10	0.23 ± 0.02	N/A	N/A
3′	1.86 ± 0.21	0.27 ± 0.03	0.20	2.5

[a] **1**, **2**, and **3**: as-is grafted layers, PS-PBA. **1′**, **2′**, and **3′**: corresponding PS-PAA brushes after hydrolysis. [b] Estimated from molecular weight and grafted amount according to the known equations as discussed in a previous publication (ref 38).

Results and Discussion

Surface Morphology of PS-PBA Brush Layers. The layer thickness for all brushes did not exceed 2.8 nm in both initial and hydrolyzed states with brushes **1** and **2** having smaller thicknesses (Table 1). Evaluation of the grafting parameters in the dry state showed medium grafting density with the average distance between the neighboring molecules of 2.5−3.6 nm (Table 1). This indicates that, under the condition of a bad solvent (air), both flexible arms collapse and form a dry layer with the vertical dimension well below the contour length (∼6−10 nm for different arms). Figure 2 shows the surface morphology of the grafted PS−PBA brushes before hydrolysis and after treatment with nonselective good solvent for both arms (toluene). AFM images obtained for large surface areas up to 20−30 μm across revealed a high quality of grafted layers with a smooth surface and the absence of microscopic inclusions generated by the grafting process or external impurities. Both surface topography and phase shift showed only very low fluctuations as can be seen in cross sections presented in Figure 3. The roughness of all grafted layers fabricated here did not exceed 0.3 nm within the 10 × 10 μm surface area that indicates molecularly smooth surfaces.

The water contact angle of the PS-PBA brush surfaces after toluene treatment was close to 80° with the lowest value

(24) Rohr, T.; Ogletree, D. F.; Svec, F.; Frechet, J. M. *Adv. Funct. Mater.* **2003**, *13*, 264−270.
(25) Birstein, T. M.; Amoskov, V. M. *Polym. Sci.* **2000**, *C42*, 172−207.
(26) (a) de Gennes, P. G. *Macromolecules* **1980**, *13*, 1069−1075. (b) Halperin, A.; Tirrell, M.; Lodge, T. P. *Adv. Polym. Sci.* **1992**, *100*, 31−71. (c) Klein, J. *Annu. Rev. Mater. Sci.* **1996**, *26*, 581−612. (d) Wittmer, J.; Johner, A.; Joanny, J. F. *Colloids Surf., A* **1994**, *86*, 85−89. (e) Julthongpiput, D.; LeMieux, M.; Tsukruk, V. V. *Polymer* **2003**, *44*, 4557−4562. (f) Lemieux, M.; Minko, S.; Usov, D.; Stamm, M.; Tsukruk, V. V. *Langmuir* **2003**, *19*, 6126−6134.
(27) (a) Singh, C.; Pickett, G. T.; Balazs, A. C. *Macromolecules* **1996**, *29*, 7559−7567. (b) Singh C.; Pickett, G. T.; Zhulina, B.; Balazs, A. C. *J. Phys. Chem. B* **1997**, *101*, 10614−10621.
(28) (a) Sidorenko, A.; Minko, S.; Schenk-Meuser, K.; Duschner, H.; Stamm, M. *Langmuir* **1999**, *15*, 8349−8355. (b) Kiriy, A.; Gorodyska, G.; Minko, S.; Jaeger, W.; Stepanek, P.; Stamm, M. *J. Am. Chem. Soc.* **2002**, *124*, 13454−13462. (c) Minko, S.; Patil, S.; Datsyuk, V.; Simon, F.; Eichhorm, K.; Motornov, M.; Usov, D.; Tokarev, I.; Stamm, M. *Langmuir* **2002**, *18*, 289−296. (d) Zhao, B.; Brittain, W. J. *J. Am. Chem. Soc.* **1999**, *121*, 3557−3558. (e) Zhao, B.; Brittain, W. J.; Zhou, W.; Cheng, S. Z. D. *J. Am. Chem. Soc.* **2000**, *122*, 2407−2408. (f) Sedjo, R.; Mirous, B.; Brittain, W. J. *Macromolecules* **2000**, *33*, 1492−1493. (g) Ruths, M.; Johannsmann, D.; Rühe, J.; Knoll, W. *Macromolecules* **2000**, *33*, 3860−3870.
(29) (a) Huck, W. T. S.; Stroock, A. D.; Whitesides, G. M. *Angew. Chem., Int. Ed.* **2000**, *39*, 1058−1061. (b) Prucker, O.; Naumann, C. A.; Rühe, J.; Knoll, W.; Franck, C. W. *J. Am. Chem. Soc.* **1999**, *121*, 8766−8770. (c) Prucker, O.; Rühe, J. *Macromolecules* **1998**, *31*, 592−610. (d) Koutsos, V.; van der Vegte, E. W.; Hadziioannou, G. *Macromolecules* **1999**, *32*, 1233−1236. (e) Koutsos, V.; van der Vegte, E. W.; Pelletier, E.; Stamouli, A.; Hadziioannou, G. *Macromolecules* **1997**, *30*, 4719−4726.
(30) Zhao, B.; Brittain, W. J. *Prog. Polym. Sci.* **2000**, *25*, 677−710.
(31) (a) Soga, K. G.; Zuckermann, M. J.; Guo, H. *Macromolecules* **1996**, *29*, 1998−2005. (b) Brown, G.; Chakrabarti, A.; Marko, J. F. *Europhys. Lett.* **1994**, *25*, 239−244. (c) Müller, M. *Phys. Rev. E* **2002**, *65*, 030802.
(32) Lemieux, M.; Usov, D.; Minko, S.; Stamm, M.; Shulha, H.; Tsukruk, V. V. *Macromolecules* **2003**, *36*, 7244−7255.
(33) Zhulina, E.; Balazs, A. C. *Macromolecules* **1996**, *29*, 2667−2673.
(34) Williams, D. R. M. *J. Phys. II* **1993**, *3*, 1313−1318.
(35) Teng, J.; Zubarev, E. R. *J. Am. Chem. Soc.* **2003**, *125*, 11840−11841.
(36) Julthongpiput, D.; Lin, Y.-H.; Teng, J.; Zubarev, E. R.; Tsukruk, V. V. *Langmuir* **2003**, *19*, 7832−7836.

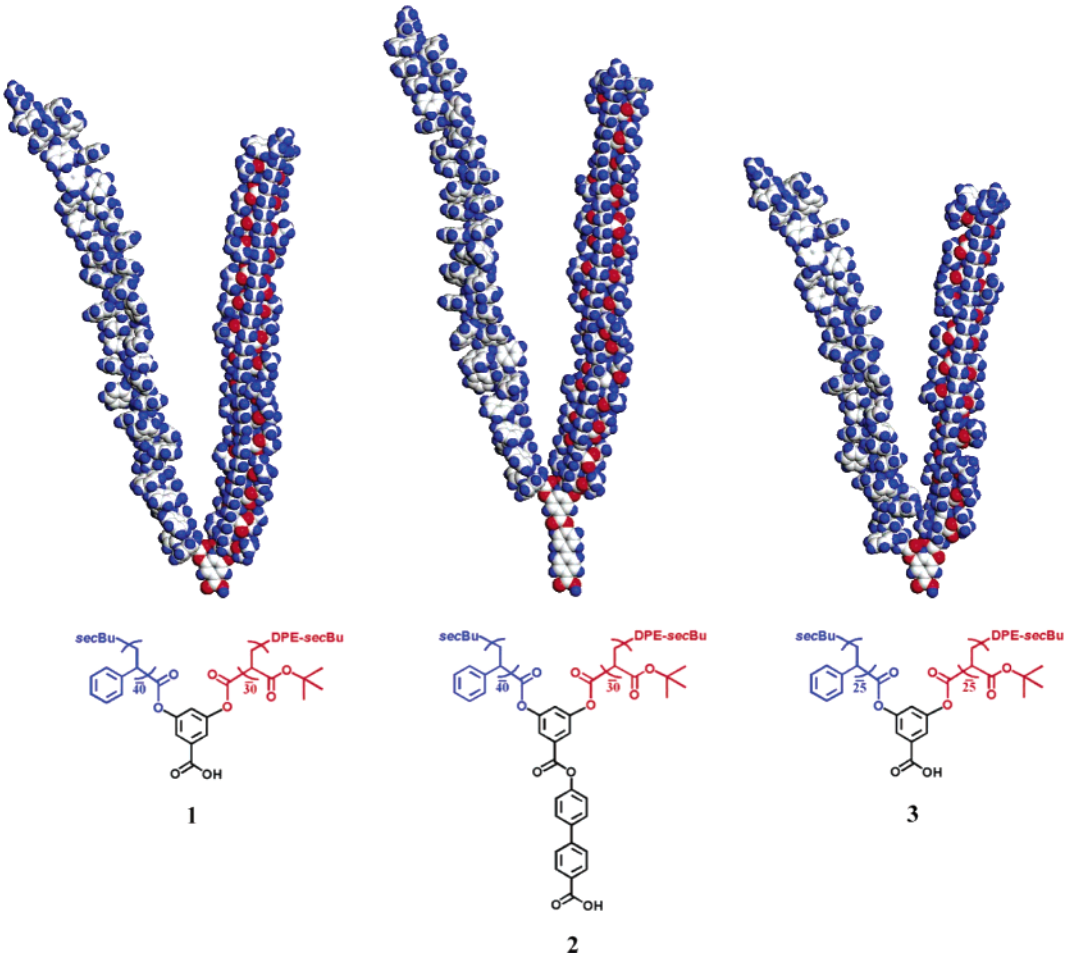

Figure 1. Chemical structure and molecular graphics representation of Y-shaped block copolymers with a short (**1**, **3**) and a long (**2**) aromatic functional stem. Molecules **1** and **2** contain 40 and 30 monomeric units, and molecule **3** contains 25 and 25 monomeric units in PS and PBA arms, respectively.

Table 2. Contact Angles of PS-PBA and PS-PAA Y-Shaped Brushes after Different Solvent Treatments

brush	PS-PBA after toluene treatment (deg)	PS-PAA after toluene treatment (deg)	PS-PAA after water treatment (deg)
1	84 ± 3	73 ± 3	53 ± 1
2	81 ± 2	76 ± 3	52 ± 2
3	77 ± 2	61 ± 1	52 ± 2

observed for brush **3** (Table 2). These values indicated a fairly hydrophobic surface as expected for the components of the PS-PBA Y-shaped molecules (90° and 80° for PS and PBA,[37] respectively). The lower value of the contact angle observed for brush **3** was caused by a higher content of PBA arms (Table 2). Therefore, the surfaces of all initial brushes studied before hydrolysis were predominantly composed of terminal flexible chains, which completely screened underlying epoxy-terminated SAM (contact angle within 50−60°).

All grafted layers possessed a very smooth surface on a microscale as well (Figures 3−5). Slight grainy topography and a uniform phase shift were observed on high-resolution AFM images. The surface roughness estimated within 1 mm^2 area was close to 0.2 nm for all PS-PBA layers. The lateral sizes of poorly developed domain morphology did not exceed 10−20 nm.

These data indicated that all PS-PBA brushes within grafted layers possessed a very weak segregation state of dissimilar arms unlike conventional mixed brushes, which usually demonstrate characteristic, well-developed microphase-separated surface morphology with dimensions of different phases reaching hundreds of nanometers across.[32] Although the dimensions of the phase-separated domain structures should be controlled by molecular weight, even for low molar mass PS-PBA mixed brushes studied earlier, domain sizes of clear, two-phase surface morphology approached a hundred nanometer range.[39] Apparently, the confinement of dissimilar arms caused by covalent attachment to the same grafting point plays a critical role in the suppression of the microscopic phase separation and defines the overall surface morphology. This, along with the shorter length of the molecular chains, is responsible for the weak segregation state of the Y-shaped brushes before the hydrolysis.

Surface Morphology of PS-PAA Brush Layers. The thickness of the grafted layers after the hydrolysis naturally decreased for all brushes and most significantly for brush **1** and **3** with a shorter stem (Table 1). The surface microughness increased but still remained very low (below 0.7 nm). A modest increase in the phase contrast was also observed for all brush layers after the hydrolysis (Figures 3−5). The surface of the

(37) Mengel, C.; Esker, A. R.; Meyer, W. H.; Wegner, G. *Langmuir* **2002**, *18*, 6365−6372.
(38) Luzinov, I.; Julthongpiput, D.; Malz, H.; Pionteck, J.; Tsukruk, V. V. *Macromolecules* **2000**, *33*, 1043−1048.
(39) Julthongpiput, D.; LeMieux, M. C.; Bergman, K. N.; Tsukruk, V. V. *Polym. Mater. Sci. Eng.* **2003**, *89*, 342−343.

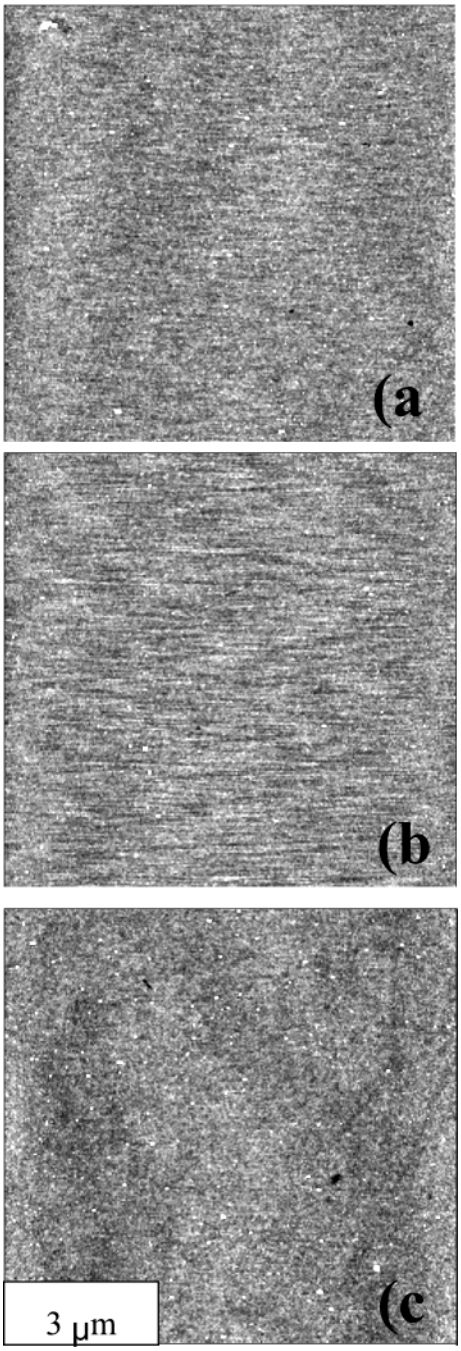

Figure 2. Large scale AFM topographical images (10 × 10 μm) of the grafted layers of PS-PBA Y-shaped molecules **1** (a), **2** (b), and **3** (c) after toluene treatment (z range is 5 nm).

amphiphilic PS-PAA brushes was covered with densely packed islands, which were more pronounced than in PS-PBA grafted layers. Their lateral dimensions were close to 10 nm as estimated after correction for the tip dilation. The height of these islands was within 1−2 nm as estimated from the topographical cross sections. Similar surface morphologies were observed for all brushes with slightly higher surface heterogeneity observed for brush **3** with an even chemical composition (PS_{25}-PAA_{25}). All of these changes of surface parameters reflected higher heterogeneity of the surface composition caused by the appearance of hydrophilic PAA arms along with hydrophobic PS arms.

The contact angle decreased by 5−16° after the hydrolysis and the subsequent toluene treatment, indicating the presence of a small amount of the hydrophilic component in the hydrolyzed brushes. The most significant decrease was detected for brush **3** that is consistent with the highest content of PAA chains in this system (Table 2). The values of the contact angle for the Y-shaped brushes were close to that expected for the PS-enriched hydrophobic surface with the presence of 15−27% of PAA chains as estimated from the Cassie−Baxter equation.[40] The contact angle for PAA chains was taken in the range of 20−40° as measured in different studies.[41]

We suggest that the surface morphology observed for the grafted layers after the hydrolysis and the following toluene treatment (selective solvent for PS arms) corresponds to an internally segregated "pinned micellar" structure theoretically predicted for sparse brushes of Y-shaped copolymers containing incompatible arms.[7] Considering that toluene is a good solvent for PS and a bad solvent for PAA, we further suggest that the topmost surface layer is predominantly composed of low surface energy PS arms, which form "coronas" of pinned micelles, whereas collapsed PAA arms constitute their "cores". This model can be suggested for the brush layer from molecules **1** and **2** with 60% of PS chains. For the brush layer from molecule **3** with an even composition, a more heterogeneous surface should be expected because of an insufficient amount of PS chains in the layer to cover the surface completely. In fact, all experimental evidence such as higher phase contrast, higher surface microroughness, and lower contact angle value for this brush layer supported this suggestion.

Switching of Surface Morphology. Conventional binary brush layers are known for their ability to change microstructure and properties under the influence of selective solvents.[32,43] Therefore, we treated Y-shaped PS-PAA brushes with water, which is a selective solvent for hydrophilic PAA arms, and observed corresponding changes of surface morphology. In fact, this treatment caused dramatic surface reorganization, leading to the formation of novel surface morphology (Figure 6). An array of craterlike nanoscale features was observed for both short and long stem Y-shaped brushes after water treatment. The craters represent discrete objects whose rims were slightly elevated with respect to their surroundings (see high-resolution 3D images and the corresponding cross sections in Figure 7). This surface morphology was the most developed for brush **2** with uneven arm composition and a long biphenyl stem with crater rims elevated by 1−1.5 nm above the surrounding matrix.

This is due to a higher grafting density and better intralayer ordering facilitated by a longer rigid stem combined with asymmetric arms. For brush **3** with an even and shorter length of dissimilar arms and a shorter stem, this craterlike morphology with rims elevated by only 0.2−0.5 nm was only barely visible under hard tapping conditions. This type of morphology has not been previously observed in binary grafted layers such as mixed or diblock hydrophilic−hydrophobic brushes. It is worth noting that the AFM tip is responsible for specific artificial

(40) Cassie, A. B. D.; Baxter, S. *Trans. Faraday Soc.* **1944**, *40*, 546−551.
(41) (a) Matyjaszewski, K.; Miller, P. J.; Shukla, N.; Immaraporn, B.; Gelman, A.; Luokala, B. B.; Siclovan, T. M.; Kickelbick, G.; Vallant, T.; Hoffmann, H.; Pakula, T. *Macromolecules* **1999**, *32*, 8716−8724. (b) Houbenov, N.; Minko, S.; Stamm, M. *Macromolecules* **2003**, *36*, 5897−5901.
(42) Sarid, D. *Scanning Force Microscopy*; Oxford University Press: New York, 1991.
(43) Minko, S.; Müller, M.; Usov, D.; Scholl, A.; Froeck, C.; Stamm, M. *Phys. Rev. Lett.* **2002**, *88*, 035502.

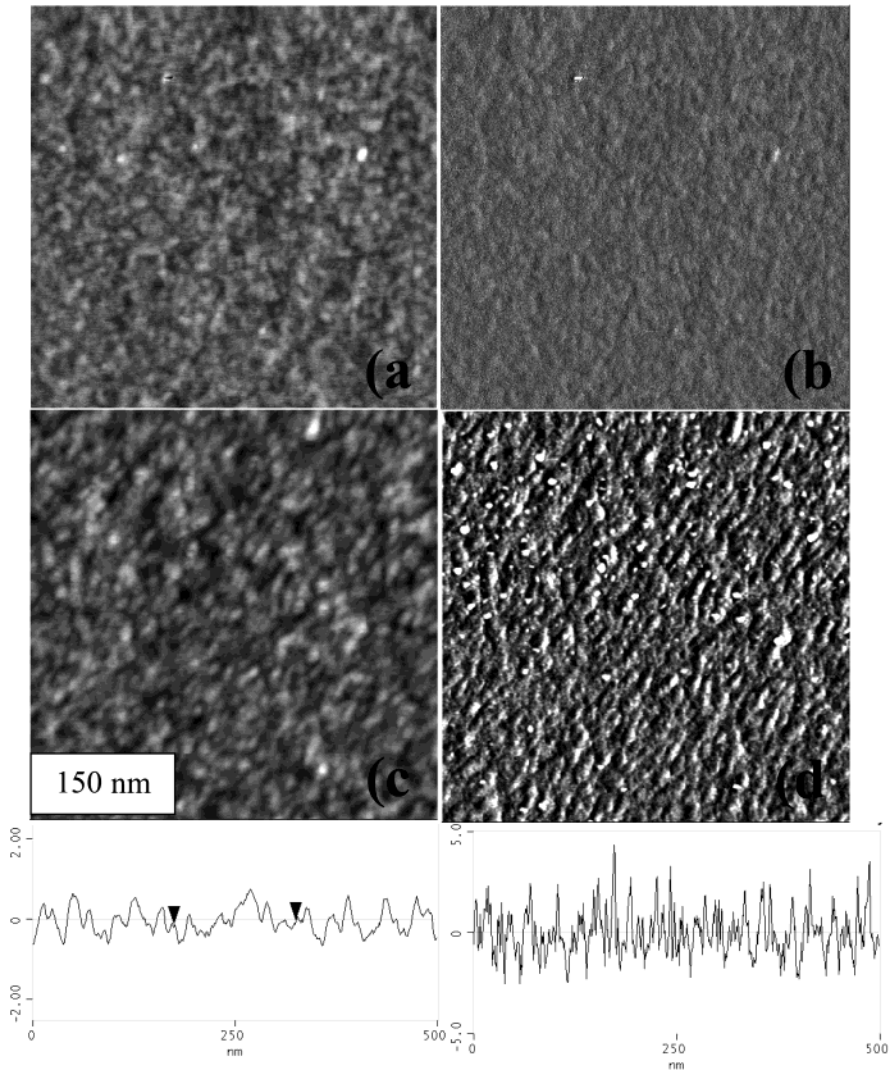

Figure 3. High-resolution AFM topographical (left) and phase (right) images (500 × 500 nm) of the grafted layers of the Y-shaped molecules **1** before (a, b) and after hydrolysis and the subsequent toluene treatment (c, d). Surface cross sections are shown for the grafted layers after hydrolysis. Vertical scales are 5 nm and 10°.

phenomena while scanning these nanoscale objects. Several most noticeable examples are clearly visible on the high-resolution AFM images (Figure 6).

First, the depth of the craters is evaluated to be at least 0.5 nm, although this parameter cannot be estimated accurately because of the tip dilation. The apparent overall lateral dimension of these features is within 20−30 nm due to the tip dilation as well. In addition, an overall shape of the central portion of the craters is obviously affected by instabilities between the AFM tip and the elevated surface features with a suddenly changing surface composition and contact area. Therefore, a precise estimation of the depth and the fine shape of these surface features is impossible. However, as known, the distance between the edges of a rim can be estimated correctly from AFM images because it is not disturbed by the tip dilation.[42]

The average diameter of the craterlike structures was within 8−10 nm for all brushes as estimated by the averaging of at least 10 independent measurements for a randomly selected array of craters as shown by various markers in Figure 7. Considering experimental observations, we suggest that this characteristic surface structure formed upon treatment with a good solvent for PAA arms (water) is composed of a collapsed central core enriched with PS arms surrounded by swollen PAA chains (see next section for detailed elaboration). For this structure, surface exposure of PAA arms should increase the hydrophilicity that was, indeed, confirmed by a significant decrease in the contact angle value to 52° for all brushes (Table 2).

This value indicates that from 65% to 90% of the surface had to be occupied by PAA arms as calculated from the Cassie equation. Therefore, a majority of the brush surface in this state is covered by the hydrophilic PAA arms with a minor amount of surface-exposed PS arms. The minimum changes of the surface wettability were observed for brush **3** as can be expected for an even composition of flexible arms with no significant preference in a volume fraction of either hydrophobic or hydrophilic chains.

To test the limits of the surface reorganization of the amphiphilic Y-shaped brushes, we conducted an additional study with solvent treatment. It can be expected that the treatment of this surface morphology with the mixed solvent, good for both PS and PAA arms, should lead to additional swelling of PS cores within the craterlike structures and, thus, the disappearance of this collapsed structure. In fact, for all brushes, we observed an increase in both lateral and vertical dimensions of the surface

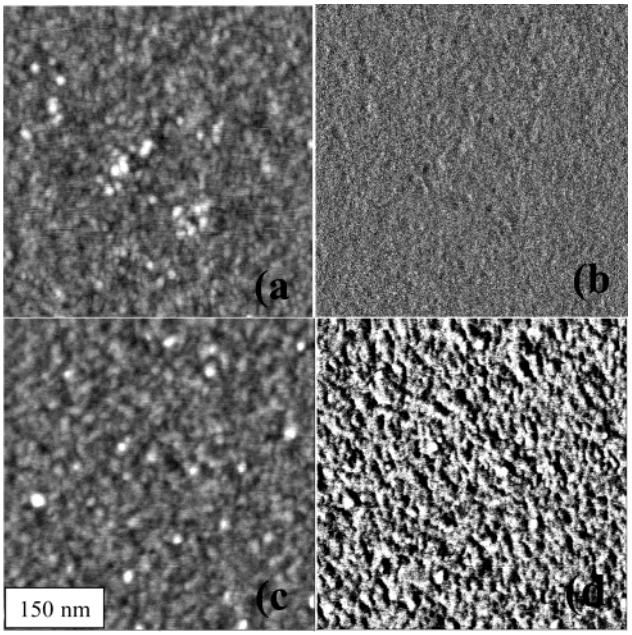

Figure 4. High-resolution AFM topographical (left) and phase (right) images (500 × 500 nm) of the grafted layers of the Y-shaped molecules **2** before (a, b) and after hydrolysis and the subsequent toluene treatment (c, d). Vertical scales are 5 nm and 10°.

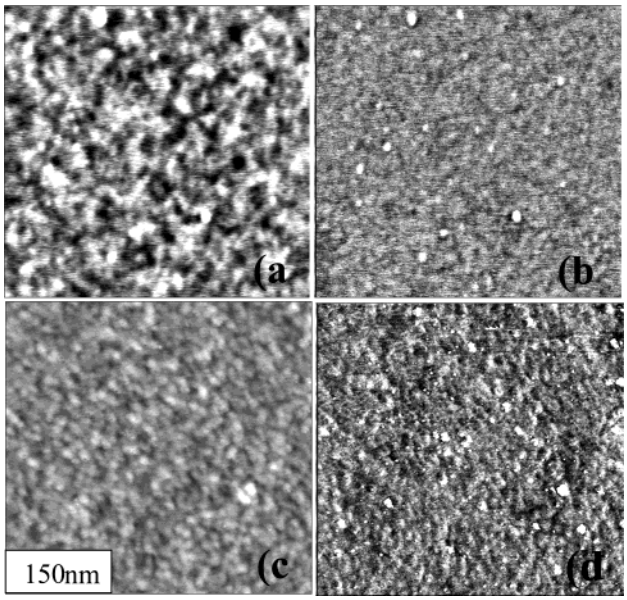

Figure 5. High-resolution AFM topographical (left) and phase (right) images (500 × 500 nm) of the grafted layers of the Y-shaped molecules **3** before (a, b) and after hydrolysis and the subsequent toluene treatment (c, d). Vertical scales are 5 nm and 10°.

structures with a conventional domain morphology replacing the craterlike morphology observed after water treatment (Figure 8). Swelling of the domain structure was much more pronounced for brushes **1** and **2** as expected for compounds with a higher content of PS phase (60%).

Models of Nanoscale Structures. Molecular simulation provides an additional insight into the structure of the Y-shaped PS-PAA brushes under different conditions and can verify our suggestions based on the AFM data discussed above. Complete molecular modeling was conducted for brush **1** with 60% of the PS chains and the grafting parameters shown in Table 1. Considering the experimental data for the grafting density and

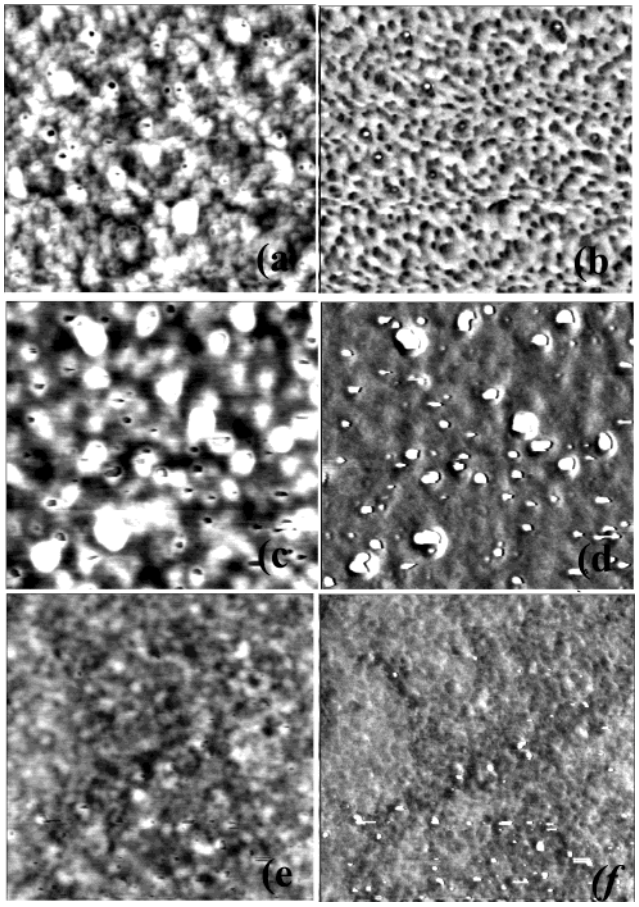

Figure 6. High-resolution AFM topographical (left) and phase (right) images (300 × 300 nm) of the grafted layers of the Y-shaped molecules **1** (a, b), **2** (c, d), and **3** (e, f) after hydrolysis and the subsequent water treatment. Vertical scales are 5 nm for a,c and 10 nm for e and 20° for all phase images.

the chemical composition of brush **1** (40 units in PS and 30 units in PAA arms), the molecular reconstruction can be conducted as illustrated in Figure 9. From the general theoretical consideration of the behavior of polymer chains tethered to a solid surface, it is reasonable to expect that in the presence of a nonselective solvent, the Y-shaped molecules would adopt the extended conformation with all arms stretching away from the substrate (Figure 9b).[1] As the quality of the solvent for one type of the arms is reduced, they would collapse and form a core of a pinned surface micelle (Figure 9a). The average diameter (d) of such micelles estimated from the AFM cross-sectional profiles was about 10 nm. Thus, the area it occupies is $\pi(d/2)^2 \approx 78$ nm^2, assuming a circular shape of the surface structures. This allows us to estimate the average number of molecules in one micelle because it can be expressed as $N = A/s$, where A is the area per micelle and s is the area per one molecule.[6] Because the experimental grafting density for PS_{40}-PAA_{30} brush **1** is one molecule per 10 nm^2 (Table 1), one micelle contains on average 7.8 grafted molecules as depicted in our model (Figure 9b).

For the sake of simplicity, we considered seven molecules, six of which were placed in the corners of a hexagon and one in its center. The average distance between the neighboring grafting points of 3−4 nm was determined experimentally (Table 1). We therefore modeled the brush as a set of Y-shaped molecules placed 3.5 nm apart in a hexagonal lattice (Figure

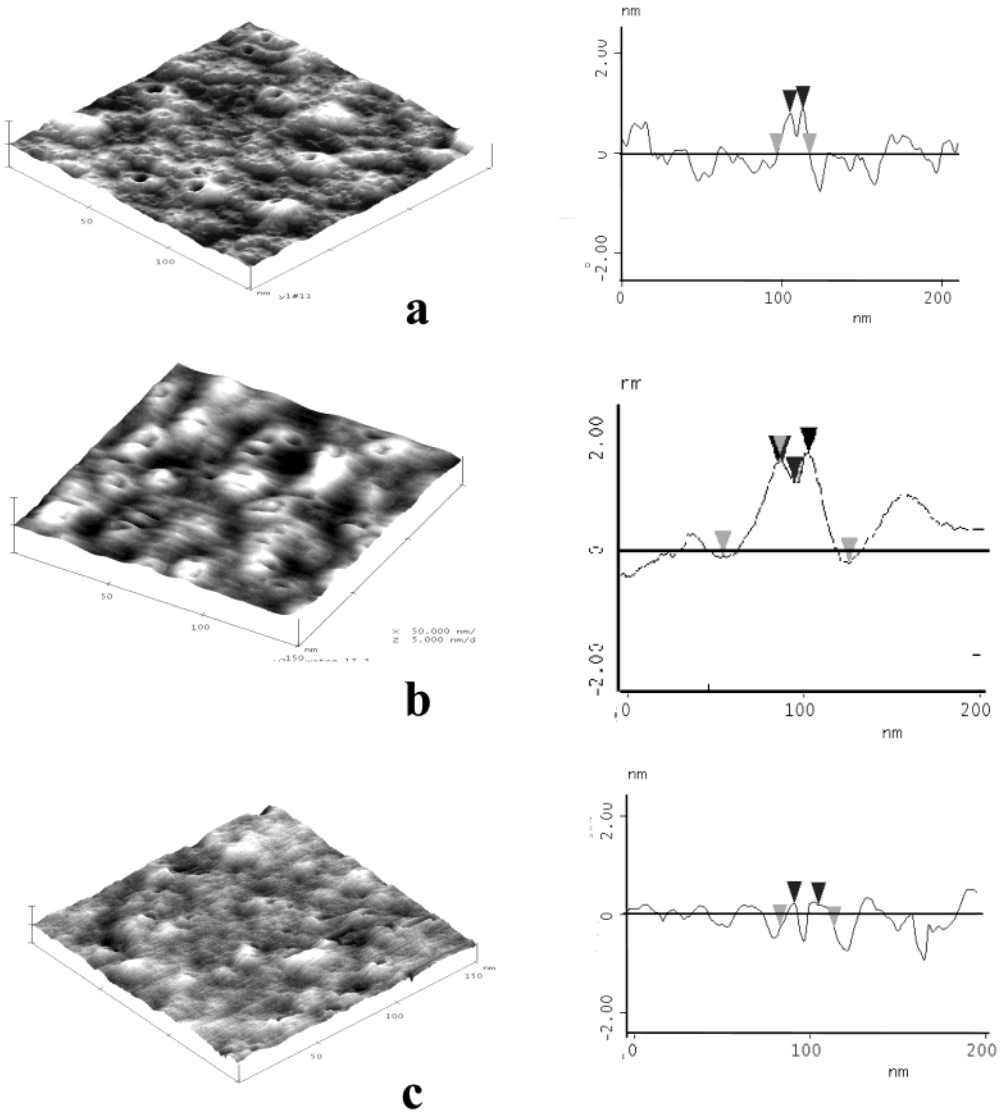

Figure 7. High-resolution 3D AFM images (150 × 150 nm) of craterlike surface micellar structures of the grafted layers of the Y-shaped molecules **1** (a), **2** (b), and **3** (c) and the corresponding cross sections. *Z* scale is 10 nm for brush **1** and **2** and 6 nm for brush **3**.

9b). The collapse of seven PAA arms upon treatment with toluene should result in the formation of a dense core in the center of a hexagon corresponding to one pinned micelle. At the same time, seven PS arms would form the micelle's corona as represented in Figure 9a. Force field minimization of this micelle with constrained atomic coordinates of 3,5-dihydroxybenzoic acid stem reveals that PS arms can cover nearly all of the area occupied by the PAA core because the volume fraction of PS arms is about 60%. In contrast, when similar modeling is done for a reverse micelle (in a good solvent for PAA), the full coverage of bulkier PS core with PAA chains cannot be completed. In this case, energy minimization drives a localization of PAA arms on the outer walls of the micelle with a central, noncovered area, revealing the PS core (Figure 9c). This model is consistent with the observed craterlike morphology, grafting parameters, and the surface composition of both Y-shaped brushes **1** and **2**. On a larger scale, an array of pinned micelles undergoing structural reorganization into craterlike micelles caused by changes in solvent quality can be simulated with molecular modeling as presented in Figure 10. In these models, different chains are color-coded (PS blue, PAA red), indicating that, indeed, the initial surface after toluene treatment can be completely covered with PS chains. Contrary, the formation of reverse surface micelles with a craterlike shape (Figure 9c) resulted in inevitably heterogeneous morphology composed of an array of nanoscale structures tethered to the solid substrate (Figure 10).

Unlike pinned micellar structures, the craterlike morphology has not been predicted theoretically for Y-shaped brushes.[7] It is also qualitatively different from the "dimple" morphology predicted and found in mixed binary brushes, inasmuch as the observed craters are spatially isolated and do not fuse into a continuous matrix.[43] Several reasons may account for this unusual morphology. The smaller volume fraction of PAA arms (40%) can facilitate such clustering. Alternatively, the interactions between PAA and the silicon surface can be strong enough to prevent conformational rearrangements of some arms and keep them permanently in the immediate vicinity of the hydrophilic substrate. The short length of both arms might contribute to such clustering as well. Finally, the Y-shaped molecular architecture imposes conformational constraints limiting micro- or macrophase separation. Regardless of what the origin of the craterlike morphology is, one simple conclusion is obvious. It exhibits structures with truly nanoscale lateral

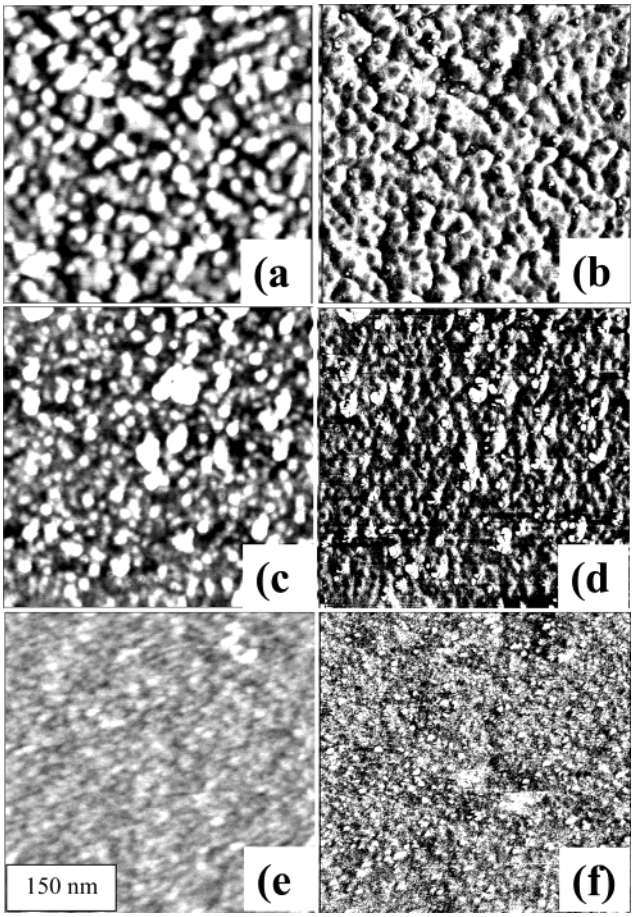

Figure 8. High-resolution AFM topographical (left) and phase (right) images (500 × 500 nm) of the grafted layers of the Y-shaped molecules **1** (a, b), **2** (c, d), and **3** (e, f) after mixed solvent treatment (chloroform/methanol 50:50 vol.). Vertical scales are 10 nm and 10°.

dimensions, which are much smaller than those found in mixed and diblock copolymer brushes.[2,4,44]

It is important to emphasize that the size of the surface micelles is directly dependent on the length of the arms of the grafted Y-shaped molecules. Because that length is within 8−10 nm in molecules **1** and **2**, the size of the surface morphological features has to be similar to that value and cannot significantly exceed it. We conclude that the combination of both the short length of the arms and the Y-shaped molecular architecture is primarily responsible for the observed nanostructured surface morphology. This is in stark contrast to mixed binary brushes containing much longer polymer chains which lead to microphase separation and, as a result, much larger surface structures. Therefore, if nanostructures are to be realized in polymer brushes, they should not have high molecular weight chains, which in many cases is considered to be an important synthetic target.

Dynamics of Switchable Surface Properties. Finally, the dynamics of switching of the surface properties caused by structural reorganizations revealed by AFM observations discussed above was studied by monitoring changes of the contact angle value after repeatable treatments with selective solvents. Figure 11 shows the contact angle values for all PS-PAA brushes after toluene and water treatments as a function of a treatment time along with corresponding droplet shape in the limiting states. The value of the contact angle after toluene treatment gradually reached 82 ± 3° for brushes **1** and **2** within the first 100 min and stayed virtually constant even after 10 h of solvent exposure.

The maximum achievable contact angle for brush **3** was slightly lower, which is due to a lower content of hydrophobic PS chains. The contact angle of all brushes decreased sharply within the first 100 min after water treatment and gradually reached a similar level of 52 ± 3° for all brushes within several hours, completing a full cycle (Figure 11). These cycles of the continuous change of the surface wettability are similar for all brush layers and can be reproduced repeatedly without deterioration of the polymer layers. These results indicate that the nanoscale structural reorganization discussed above can control, consistently and efficiently, macroscopic wetting properties of the amphiphilic Y-shaped brushes.

Conclusions

In conclusion, we fabricated and characterized novel Y-shaped brush layers chemically grafted to the silicon surface. We demonstrated that spatial constraints imposed by a covalent junction of two dissimilar (hydrophobic and hydrophilic) polymer chains with medium molecular weights in Y-shaped

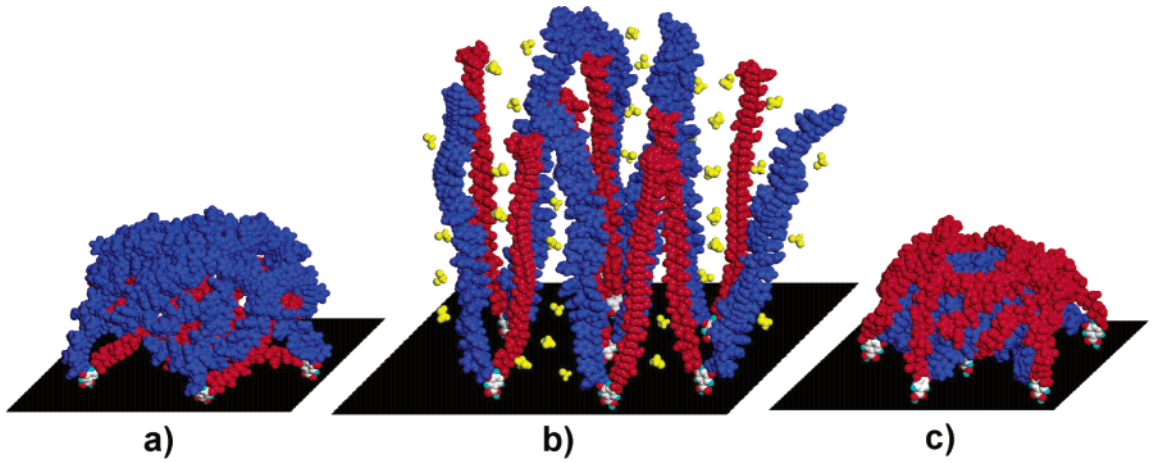

Figure 9. Molecular models of the proposed structural rearrangement in Y-shaped brushes. Internally segregated pinned micelle composed of seven grafted PS-PAA molecules spaced 3.5 nm apart. Upon treatment with toluene and the following drying, the PS arms (blue) form corona covering the micelle's core consisting of seven PAA arms (red). (b) Representation of the same seven molecules **1** swelled in a nonselective solvent (yellow). (c) Top-open craterlike structure containing seven collapsed PS arms partially covered by seven PAA chains.

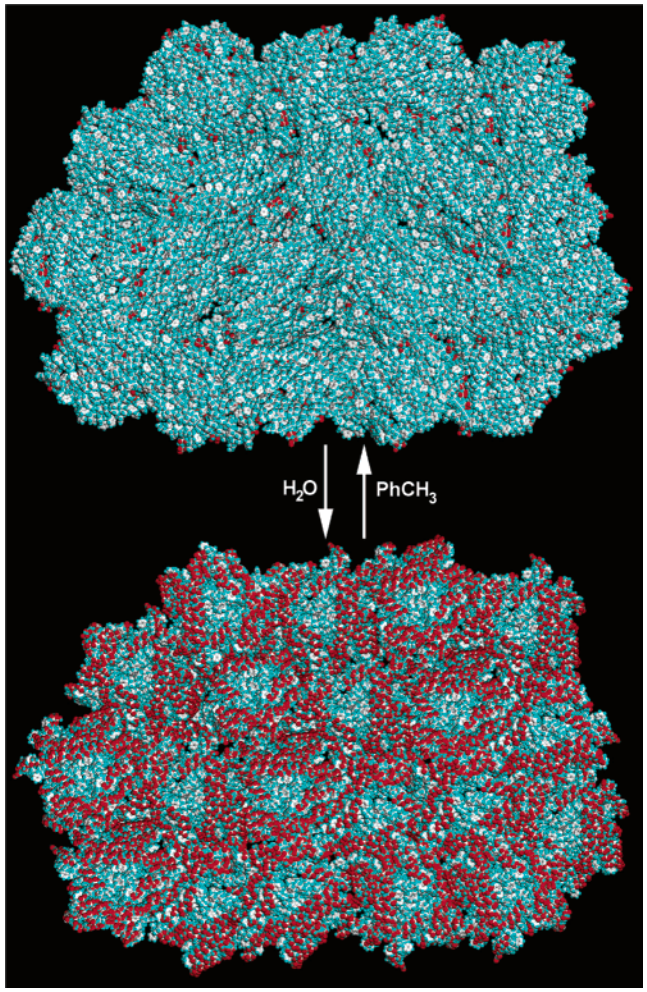

Figure 10. Molecular graphics representation (top view) of 20 surface micelles containing 140 Y-shaped molecules **1** spaced 3.5 nm apart in a hexagonal lattice. Treatment with toluene results in a complete coverage of PAA cores with PS chains (top), whereas treatment with water leads to a craterlike morphology (bottom). Hydrogen, blue; oxygen, red; carbon, white.

molecules caused the formation of a novel type of segregated surface micellar structures (pinned and craterlike), which measure only 10 nm in diameter. An array of crater-shaped nanoscale features of different contrast was observed for both short and long stem Y-shaped molecules. We concluded that the formation of such nanoscale features was mainly caused by covalent junctions of dissimilar arms to a single grafting point (Y-shaped molecular architecture) and can also be due to a relatively short length of the arms. These two features are believed to be responsible for a weak segregation state of the Y-shaped brushes before and after the hydrolysis. This type of surface morphology is very different from conventional binary grafted layers such as mixed and diblock amphiphilic brushes.

We proposed a model of segregated pinned micellar surface structures and reverse craterlike micelles featuring different segregation states of PS and PAA arms of a core−shell type. The microstructure suggested on the basis of AFM results was supported by molecular modeling of the conformational states of tethered Y-shaped molecules and their aggregates. These micellar nanostructures are capable of conformational reorganization after exposure to selective solvents. These types of

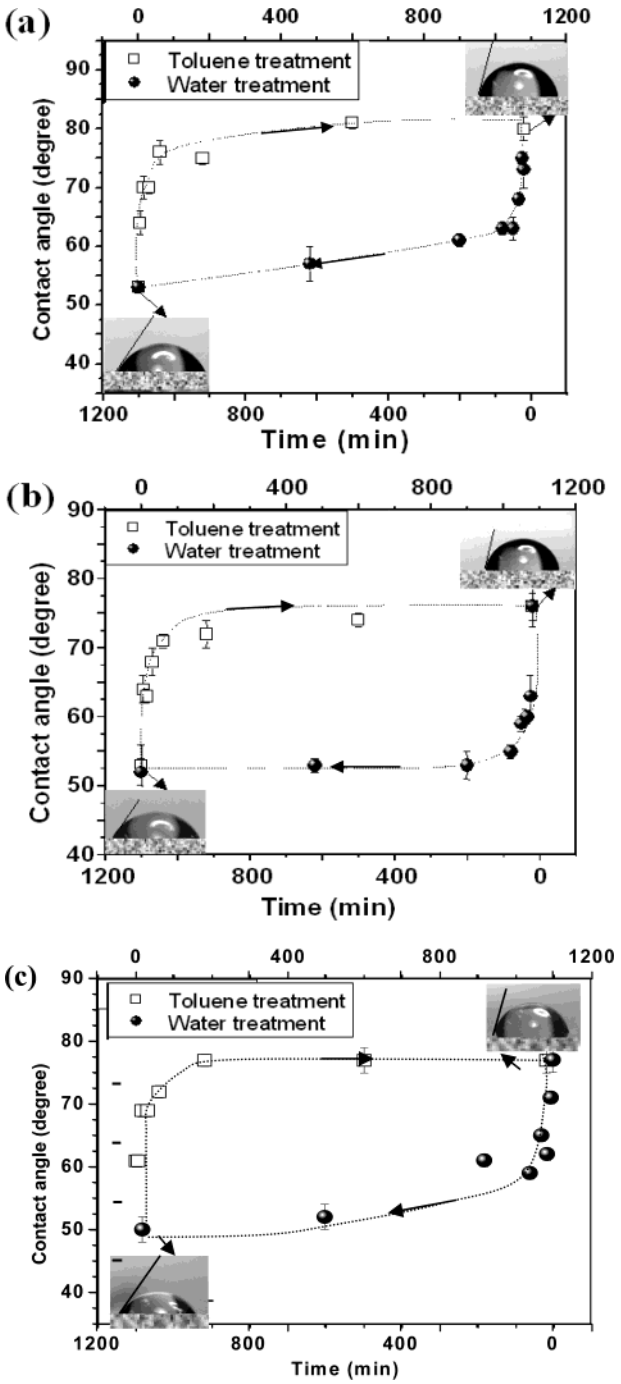

Figure 11. Cyclic dynamics of surface wetting properties (contact angle) as a function of solvent treatment time for the grafted layers of the Y-shaped molecules **1** (a), **2** (b), and **3** (c).

surface structures and switching behavior are similar for all three brushes studied here with minor variations related to changes in composition/molecular weight of flexible arms and the stem length. Switching of the surface wetting properties driven by changes in the local heterogeneous composition of Y-shaped brushes is of potential interest because the resulting nanoscale morphology of craterlike type can facilitate assembly of inorganic nanoparticles, proteins, and charged chemical species. The approach proposed here can be considered as a promising way toward the patterning of solid substrates with adaptive nanowells, which can be used for controlled and selective trapping of adsorbing nanoscale objects. We believe that the

(44) Sevick, E. M.; Williams, D. R. M. *Phys. Rev. Lett.* **1999**, *82*, 2701.

regular surface patterning on a nanoscale can be achieved in the future for these layers if the periodic conditions for grafting and lateral phase separation will be applied similarly to regular block copolymers.

Acknowledgment. We acknowledge support by the National Science Foundation, CMS-0099868 and DMR-0308982 Grants, Air Force Office for Scientific Research, F496200210205, and Grant M01-C03 from DoC through the National Textile Center. E.R.Z. acknowledges support provided by University Research Grant (URG) of Iowa State University.

Supporting Information Available: Experimental details (PDF). This material is available free of charge via the Internet at http://pubs.acs.org.

JA038051U

Supporting Information.

JA038051U

TITLE: Y-shaped Amphiphilic Brushes with Switchable Micellar Surface Structures

AUTHORS: D. Julthongpiput, Y.-H. Lin, J. Teng, E. R. Zubarev, V. V. Tsukruk**

The synthesis of the Y-shaped molecules **1-3** presented in Figure 1 is described in detail elsewhere (Table 1). Carboxyl-terminated PS (M_w=2,400; PDI=1.2) and PBA (M_w=4,200; PDI=1.2) were purchased from Polymer Source, Inc. Sequential coupling of PS and PBA to a silyl-protected 3,5-dihydroxybenzoic acid following by the deprotection of the carboxyl focal point under mild basic conditions (DMAP) gave Y-shaped copolymer **1**. The product was purified by conventional flash chromatography and had a very narrow polydispersity (1.07) and the average molecular weight of 7,300 (Figure S1).

Table 1. Molecular weight characteristics of PS-PBA Y-shaped molecules determined by GPC relative to polystyrene standards.

Brush	M_w, g/mol	M_w/M_n
1	7,300	1.07
2	7,730	1.05
3	6,520	1.08

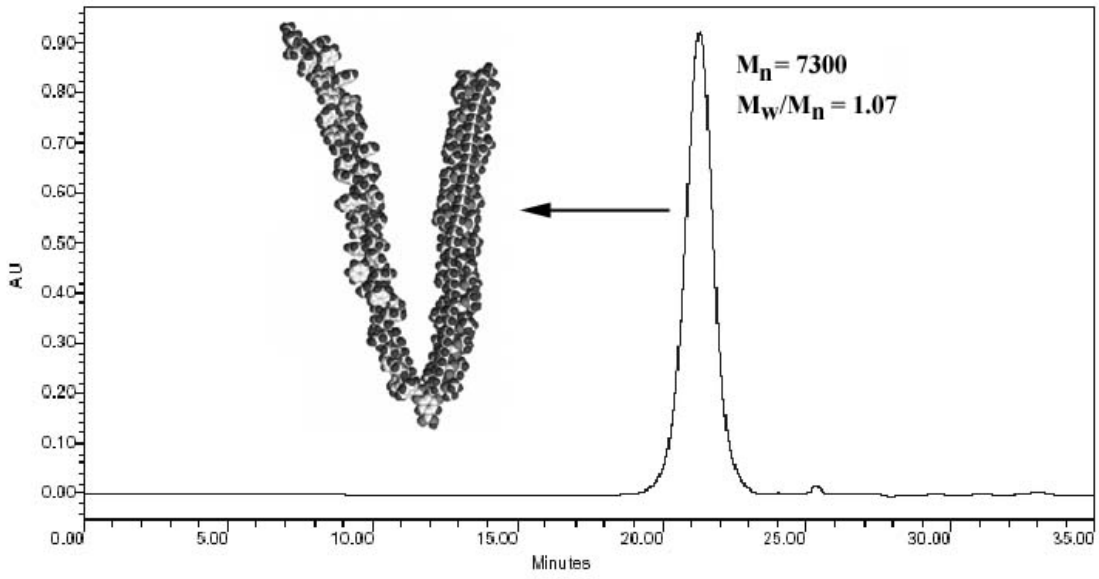

Figure S1. GPC trace of PS-PBA Y-shaped brush **1.**

That structure was converted to **2** upon esterification reaction with a hydroxybiphenyl acid silyl ester followed by the cleavage of the protecting group. The combination of biphenyl protons (7.65 and 7.92 ppm) and a signal of C*H* of the polyacrylate backbone (2.25 ppm) provided excellent internal references in ^{1}H NMR spectra which allowed us to accurately estimate the number of monomeric units in both arms (Figure S2). From NMR data, we estimated that the PS chain in molecules **1** and **2** is composed of 40 monomeric units and the PBA arm has on average 30 units. When the synthetic sequence in which the arms are attached to 3,5-dihydroxybenzoic acid changes (first PBA and then PS) the average length of both chains in the final product becomes 25 monomeric units (brush **3**). These changes are due to a partial fractionation of polymeric products upon purification on silica gel by flash chromatography. These variations give an opportunity to address the role of arms asymmetry (a volume ratio of PS and PAA arms is approximately 60:40 in molecules **1**

and **2**, and 50:50 in molecule **3**) and their length on the corresponding surface morphology.

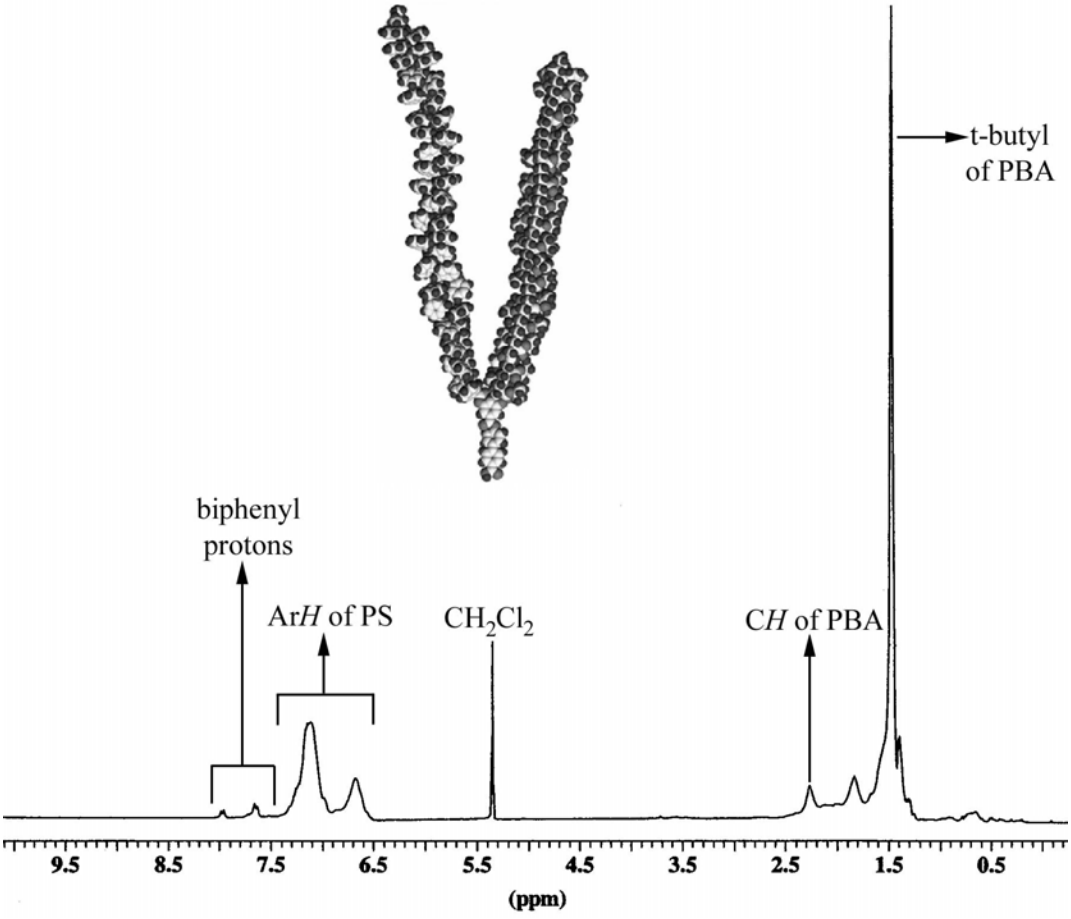

Figure S2. NMR spectrum of PS-PBA Y-shaped brush **2**.

For the fabrication of the brush layer, a "grafting to" approach from a polymer melt to the epoxy-terminated self-assembled monolayers (SAMs) has been used as discussed in detail in previous publications. The polymers were spin-coated from a 1.5% wt. toluene solution onto the wafers functionalized with the epoxysilane SAM. The thickness of the initial spin-coated film measured by ellipsometry was 30±3 nm. The coated wafers were annealed at grafting temperature of 135˚C for 6 hours to enable the end groups to graft to

the substrate. The un-grafted polymer was removed by multiple extractions with toluene and additional treatment in an ultrasonic bath. The grafted PS-PBA Y-shaped polymer brush was then hydrolyzed in the mixture of trifluoroacetic acid and tetrahydrofuran (70:30 vol.) for 48 hrs at room temperature. Complete disappearance of t-butyl groups was confirmed by ^{13}C NMR of polymers obtained in solution under identical deprotection conditions. The hydrolyzed grafted layer was rinsed with Nanopure water and toluene followed by ultrasonic bath. The samples were dried under nitrogen atmosphere and kept in sealed containers stored in a desicator prior to further studies. All grafting routines were conducted under Cleanroom 100 conditions to avoid external contaminations of highly active surfaces.

Changes in the contact angle of the grafted layers after treatment with different solvents were measured for a specimen, which was placed in a proper solution for different time periods. For an investigation of the surface reorganization of Y-shaped PS-PAA brushes, we immersed samples in three different solvents including toluene (good solvent for PS), mixed solvent of 50% methanol and 50% chloroform (nonselective solvent), and water (good solvent for PAA) for 20 hrs. Contact angles of Nanopure water were measured within 10 minutes after the solvent treatment and repeated in several hours. The values quoted in this paper are the final, stabilized values, which remain unchanged with time. To assure complete surface reorganization, treatment with water was conducted at elevated temperature of 75˚C (above the glass transition temperature for PS arms as determined by DSC (68˚C)). For a detailed investigation of the kinetic cycles, we immersed brush layers in toluene for different periods of time ranging from 5 min to 18 h. Then, the specimen was immersed in water and measurements were repeated. Each

data point was obtained for the same specimen, which was stored for a certain period time, rinsed and dried before the contact angle measurement. Such a measurement cycle was followed by a next treatment period for an additional period of time. All changes of film properties observed experimentally were completely reversible, and the switching experiments were repeated several times for each sample.

Contact angle measurements were conducted with a sessile drop method with a custom-built optical system. Film thickness was measured using a COMPEL automatic ellipsometer (InOm Tech, Inc.). The thickness of grafted layers was evaluated with a double layer fitting procedure taking into account the independently measured thickness of a silicon oxide layer (about 1.2 nm), the SAM layer measured prior to grafting, and the known refractive indices for polymer materials. All reported thickness values were averaged over six measurements collected from different locations on the substrate.

Atomic force microscopy (AFM) studies were performed on Dimension 3000 and Multimode Nanoscope IIIa microscopes (Digital Instruments, Inc.). Silicon or silicon nitride AFM tips were used with a tip radius ranging from 10 to 30 nm as tested with a gold nanoparticle reference sample. Tapping AFM imaging was used according to the well-established procedure. Scanning was conducted for scale sizes ranging from 30 μm to 300 nm across with scanning rates of 0.5 – 1 Hz under variable loading conditions (hard and light tapping modes).